Detection of internal defects applying photothermal super resolution reconstruction utilizing two-dimensional high-power random pixel patterns

by Julien Lecompagnon*, Philipp Hirsch*, Christian Rupprecht**, Mathias Ziegler*

* *Bundesanstalt für Materialforschung und -prüfung, Division 8.7: Thermographic Methods, Berlin, Germany*
** *Technische Universität Berlin, Chair of Coating Technology, Berlin, Germany*

Abstract

In this work, we report on our progress for investigating a new experimental approach for thermographic detection of internal defects by performing 2D photothermal super resolution reconstruction. We use modern high-power laser projector technology to repeatedly excite the sample surface photothermally with varying spatially structured 2D pixel patterns. In the subsequent (blind) numerical reconstruction, multiple measurements are combined by exploiting the joint-sparse nature of the defects within the specimen using nonlinear convex optimization methods. As a result, a 2D-sparse defect/inhomogeneity map can be obtained. Using such spatially structured heating combined with compressed sensing and computational imaging methods allows to significantly reduce the experimental complexity and to study larger test surfaces as compared to the one-dimensional approach reported earlier.

1. Introduction

For a long time, the rule of thumb for active thermography as a non-destructive testing method has been that the resolvability of internal defects/inhomogeneities is limited to a ratio of defect depth/defect size less or equal to one. This limit mainly originates from the diffusive nature of thermal conduction in solids. The application of the photothermal super resolution reconstruction approach has recently allowed to overcome this limit. This approach significantly improved the width-to-depth range for which internal defects can be resolved.
In previous works, it has already been shown that the mentioned classical limit can be overcome for one-dimensional and two-dimensional defect geometries by scanning the object under test (OuT) using single laser spots/lines with subsequent numerical photothermal super resolution reconstruction [1, 2, 3]. These established methods use a combination of large number of sequential spatially structured illuminations, which come at the expense of additional experimental complexity, long measurement times, large data sets, and therefore tedious numerical analysis. In this work, we report on our progress characterizing a new experimental approach to significantly reduce the experimental effort by using full-field two-dimensionally structured laser-based illumination instead of subsequent local excitations.

2. Motivation on Photothermal Super Resolution Reconstruction

The surface temperature response of an OuT, which is simplistically modeled as a thermally-thin plate, can be represented as the sum of an initial temperature distribution $T_0(x,y)$ and the spatial convolution ($*_{x,y}$) of the thermal point spread function (PSF) $\Phi_{\mathsf{PSF}}(x,y,t)$ and the heat source distribution $a(x,y)$ in a Green's function like model as follows:

$$T_{\mathsf{meas}}(x,y,z=0,t) - T_0(x,y) = \Phi_{\mathsf{PSF}}(x,y,t) *_{x,y} a(x,y) \tag{1}$$

The thermal PSF can be calculated analytically if the thermal properties of the OuT's material (specific heat capacity c_p, thermal conductivity λ, density ρ, diffusivity α) are known along with its thickness d, the coordinate centroid $(\bar{x},\bar{y})$, the thermal wave reflection coefficient R (typical $R \approx 1$) and the external heat flux Q as shown in Eq. (2) [4]. Further, it is assumed that the external heat flux Q can be split into a spatial distribution $a_{\mathsf{ext}}(x,y)$ of similar independent heat fluxes with amplitude $\hat{Q}$ and a spatial structure $I_{x,y}(x,y)$ as well as a temporal structure $I_t(t)$ according to Eq. (3).

$$\Phi_{\mathsf{PSF}}(x,y,t) = \frac{2\cdot\hat{\mathrm{Q}}}{c_p\rho(4\pi\alpha t)^{3/2}} \cdot \mathrm{e}^{\frac{(x-\bar{x})^2+(y-\bar{y})^2}{4\alpha t}} \cdot \sum_{n=-\infty}^{\infty} R^{2n+1}\mathrm{e}^{-\frac{(2nd)^2}{4\alpha t}} *_t I_t(t) \tag{2}$$

$$Q(x,y,t) = \hat{Q}\cdot I_{x,y}(x,y) *_{x,y} a_{\mathsf{ext}}(x,y) *_t I_t(t) \tag{3}$$

The overall heat source distribution $a(x,y)$ can then be represented as the sum of the deliberately applied external heat sources (i.e., the photothermal heating by the external illumination) and an internal «*apparent*»heat source distribution $a_{\mathsf{int}}(x,y)$. This latter apparent heat source distribution originates from the fact that in active thermographic testing, internal defects with lower effusivity appear in the measured surface temperature response as heat sources. This is because they impede the local heat flow in a way that the temperature rise at their respective locations appears as if there is an internal active heat source

present. This apparent internal heat source distribution therefore resembles the internal defect structure which is ultimately to be reconstructed.

$$a(x,y) = I_{x,y}(x,y) *_{x,y} \left(a_{\mathsf{ext}}(x,y) + a_{\mathsf{int}}(x,y)\right) \tag{4}$$

By performing multiple different independent measurements $m \in [1,\ldots,n_m]$ and by introducing regularizers which make use of priors related to the equation's physical nature (ℓ_2) plus the fact that the internal defect structure is constant for all measurements and defects are sparsely distributed ($\ell_{2,1}$), the solution space can be constrained such that the severely ill-posed Eq. (1) can be inverted to extract the heat source distribution $a(x,y)$ [5]. This numerical reconstruction can be performed using the alternating direction method of multipliers (ADMM) algorithm [6] leading to a reconstruction $a_{\mathsf{rec}}(x,y)$ of $a(x,y)$ and therefore the internal defect pattern as encoded in $a_{\mathsf{int}}(x,y)$:

$$\begin{aligned} &\text{minimize} \quad f(p)+g(q) = \left\|\Phi_{\mathsf{PSF}}(x,y) *_{x,y} p^m(x,y) - T^m_{\mathsf{meas}}(x,y) - T_0(x,y)\right\|_2^2 + \lambda_{21}\left\|q^m(x,y)\right\|_{2,1} + \lambda_2\left\|q^m(x,y)\right\|_2^2 \\ &\text{subject to} \quad p^m(x,y) - q^m(x,y) = 0 \end{aligned} \tag{5}$$

The reconstruction result of the internal defect pattern $a_{\mathsf{rec}}(x,y)$ can then be determined by the sum over the solution for each measurement:

$$a_{\mathsf{rec}}(x,y) = \sum_m p^m(x,y) \tag{6}$$

The relative strength of the regularizing terms can be adjusted by carefully choosing the $\lambda_{21}, \lambda_2 \in \mathbb{R}$ parameters. Currently those parameters need to be inputted by the user specifically tailored to the specific reconstruction problem at hand. Determining a suitable set of set of regularizing parameters automatically prior to reconstruction is currently subject of current research.

3. Two-dimensional Random Pixel Pattern Excitation

The recent developments in the field of digital micromirror device (DMD)-based high-power laser projectors now allow for their application within active thermographic testing. With such projectors, it is possible to project whole pixel patterns at once, which reduces the amount of measurements required to achieve homogeneous illumination of the test object on average and thus shortens the measurement time [7]. Although the available projectors feature high independent pixel counts ($\approx 10^6$), their still rather low optical output irradiances of $< 20\,\mathrm{W\,cm^{-2}}$ make it necessary to group the available pixels into larger pixel clusters in order to achieve a sufficient SNR. The influence of this clustering of pixels into larger pixel clusters with side length d_{spix} on the achievable reconstruction result has been already investigated in a previous work [8].

A representative photothermal super resolution reconstruction measurement using multiple 2D random pixel patterns as illumination source can be seen in figure 1 [7].

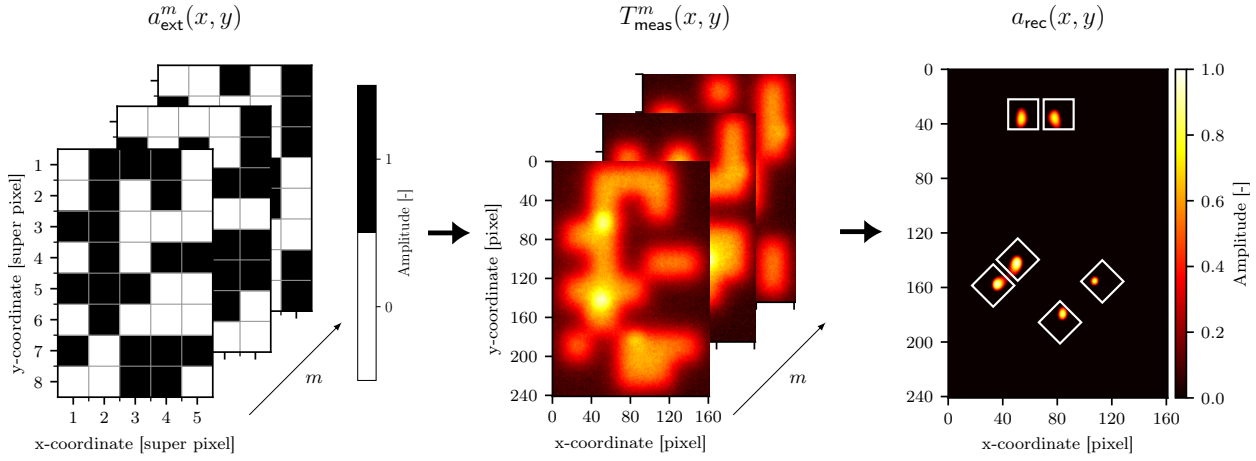

Fig. 1. *Simplified flow chart for two-dimensional random pattern excitation photothermal super resolution reconstruction: The left image shows the illumination pattern a^m_{ext} for a 2D random pixel-pattern illumination with a 5×8 grid of pixel clusters with a fill factor of $\beta = 0.5$, the corresponding T^m_{meas} measured surface temperature signal is shown in the middle. On the right, the reconstructed defect pattern a_{rec} from the measured data is shown. The white boxes indicate the true defect positions.*

4. Forward Solution

One of the advantages of using a simplified model as given in Eq. (1) for representing the complex interaction of an OuT with internal defects and structured illumination lies in the fact that it is possible to find the forward solution to the stated inverse problem and solve it rather easily. This forward solution can be used to generate synthetic measurement data which in turn can be applied to investigate the influence of the experimental parameters on quality of the reconstruction result. Exemplary experimental parameters to vary could be the number of patterns projected, the size of the used pixel clusters or the fill factor of the projected patterns and more. The following candidate for a forward solution has proven to give a suitable approximation of real measured data:

$$T^m_{\mathsf{meas,\ sim}}(x,y) = \\ \Phi_{\mathsf{PSF}}(x,y) *_{x,y} \left(\underbrace{a^m_{\mathsf{pattern}}(x,y)}_{I_{x,y} *_{x,y}\ a_{\mathsf{ext}}} + \underbrace{\zeta \cdot D(x,y) \odot \left(\Phi_{\mathsf{PSF}}(x,y) *_{x,y} a^m_{\mathsf{pattern}}(x,y)\right)}_{a_{\mathsf{int}}} \right) + \mathcal{N}_{\mathsf{noise}}(x,y)\,, \tag{7}$$

where $a^m_{\mathsf{pattern}}(x,y)$ is the excitation pattern used in the measurement $m \in 1,\ldots,n_{\mathsf{patterns}}$, ζ a factor encoding the relative strength of the defect signal (encoding the depth/contrast of the defect in the bulk material), $D(x,y)$ being a binary defect map, $\odot$ is the element-wise (Hadamard) product operator and $\mathcal{N}_{\mathsf{noise}}(x,y)$ a Gaussian noise term added to model the NETD of the infrared camera.

5. Parameter Study: Number of Patterns

With the help of Eq. (7) it is possible to conduct numerical parameter studies on synthetic measurement data. In order to compare different reconstruction results quantitatively, a comparison metric is needed. For this specific purpose, the following metric has been developed condensing the reconstruction result a_{rec} to a single numerical value $C\left(a_{\mathsf{rec}}\right) \in \mathbb{R}_+$, where a smaller number indicates a better reconstruction result:

$$C\left(a_{\mathsf{rec}}\right) = \mathrm{NMSE}\left(D, a_{\mathsf{rec}}\right) + \left\| \left(1 - \eta'(x,y)\right) \odot a_{\mathsf{rec}} \right\|_2 \tag{8}$$

This metric is computed as the sum of the normalized mean square error (NMSE) of the reconstruction result and a location dependent penalty term which penalizes reconstructed false-positive defect signals far away from the actual defects more than closer ones. This term consists of the ℓ_2-norm of the element wise product of the reconstruction result with the inverted normalized penalization term $\eta^(x,y)$ which is defined as the true defect signal convolved with the PSF:

$$\eta(x,y) = D(x,y) *_{x,y} \Phi_{\mathsf{PSF}}(x,y)\,. \tag{9}$$

The use of the PSF causes this factor to take full effect for all false-positive defect signals which are further away from the true position than the spatial width of the PSF itself. On the other hand, the NMSE is defined as follows:

$$\mathrm{NMSE}\left(x_{\mathsf{true}}, x_{\mathsf{rec}}\right) = \frac{\|x_{\mathsf{true}} - x_{\mathsf{rec}}\|_2^2}{\|x_{\mathsf{true}} - \overline{x_{\mathsf{true}}}\|_2^2}\ . \tag{10}$$

With this metric it is possible to find the set of regularizing parameters $\{\lambda_{21}, \lambda_2\}$ which result in the best reconstruction result of the true defect map $D(x,y)$ by solving the following minimization problem:

$$\underset{\lambda_{21},\ \lambda_2}{\mathrm{minimize}}\ C\left(a_{\mathsf{rec}}\right)\ , \tag{11}$$

where a_{rec} is determined by solving the minimization problem stated in Eq. (5) with λ_{21} and λ_2 as inputs. In order to solve the minimization problem stated in Eq. (11), the Differential Evolution search algorithm can be used [9]. This algorithm allows to search in vast and non-linear solution spaces for a global minimum and it is very robust regarding the shape of the solution space itself. As a downside, this algorithm does not guarantee to find the global minimum within a finite amount of iterations.

6. Results

In order to learn about the influence of the number of different projected patterns n_{patterns} on the reconstruction quality $C(a_{\text{rec}}^{n_{\text{patterns}}})$, several reconstructions of simulated and measured data have been performed. For this, an OuT made of 316L stainless steel ($\alpha = 3.76 \times 10^{-6}\,\text{m}^2\,\text{s}^{-1}$, $\rho = 7950\,\text{kg}\,\text{m}^{-3}$, $c_p = 502\,\text{J}\,\text{kg}^{-1}\,\text{K}^{-1}$) has been chosen/modeled which contains several square internal defects with a side length of $d_{\text{def}} = 2\,\text{mm}$ at a depth of $0.5\,\text{mm}$ below the surface (resulting to a best fit $\zeta = 0.5$). These defects are distributed within the region of interest (ROI) with separation distances of $a_{\text{def}} \in \{0.5, 1, 2, 4\}\text{mm}$ and are oriented at $45°$ with respect to the orientation of the camera pixels in order to showcase the true two-dimensional reconstruction properties of the algorithm.

For the simulation data, the ROI has been restricted to a single defect pair simulated at separation distances of $a_{\text{def,sim}} \in \{1.5, 0.5, 0.2\}\text{mm}$. All simulations as well as the measurements have been conducted with a spatial resolution of $\Delta x, \Delta y = 0.1\,\text{mm}$. This leaves a separation of only $2\,\text{pixel}$ for the closest simulated defect pair or $5\,\text{pixel}$ for the measured data respectively. A depiction of the resulting true defect distribution within the ROI and an overview over an exemplary set of results is shown in figure 2.

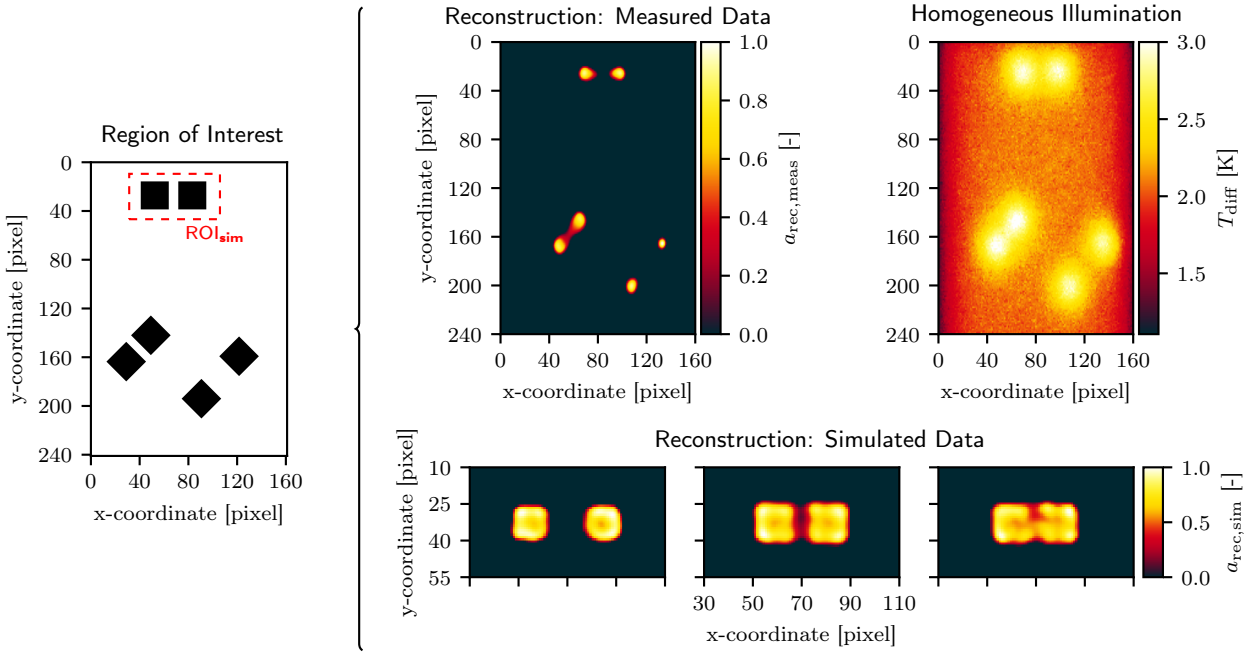

Fig. 2. *Overview over the achieved reconstruction results on measured and simulated data: For the ROI shown in the leftmost plot, several reconstruction results are shown on the right. The ROI contains several square shape defects with a side length of* $2\,\text{mm}$ *and separation distances of* $a_{def} \in \{0.5, 1, 2, 4\}\text{mm}$ *between each other. The top left reconstruction plot shows the reconstruction for measured data (*$n_{patterns} = 50$ *and* $d_{spix} = 0.4\,\text{mm}$*), while the three plots in the bottom row show a reconstruction for simulated data (*$n_{patterns} = 50$*,* $d_{spix} = 0.4\,\text{mm}$ *and* $\text{std}(\mathcal{N}_{noise}) = 0.1 \cdot \max(T_{meas,\,sim})$*) for different distances between the defects of* $a_{def,sim} \in \{1.5, 0.5, 0.2\}\text{mm}$*. The underlying input data for each reconstruction has been sampled at* $\Delta x, \Delta y = 0.1\,\text{mm}$*. For reference, in the top right plot the temperature rise* T_{diff} *of the ROI after experiencing a homogeneous illumination for a pulse length of* $t_{pulse} = 0.5\,\text{s}$*, comprising* $\hat{Q} = 87\,\text{W}$ *of radiant power, sampled at* $t_{eval} = 0.5\,\text{s}$ *and measured within the same experimental setup is shown.*

In order to examine the dependency of the reconstruction quality on the amount of patterns projected, several reconstructions on simulated measurement data for $n_{\text{patterns}} \in \{2, 4, 6, 8, 10, 16, 20, 32, 40, 50, 80, 100\}$, a cluster size of $d_{\text{spix}} = 0.4\,\text{mm}$ a pattern fill factor of $\beta = 0.5$ and three different defect separation distances have been performed. For evaluating this 36 data points and finding the corresponding best set of regularizing parameters the minimization problem stated in figure 5 has been solved $\approx 25\,000$ times (at a rate of $8 - 30\,\text{s}$/reconstruction on modern high performance computer hardware). A resulting graph summarizing the dependence of the number of projected patterns on the reconstruction quality is shown in figure 3.

In the semilogarithmic depiction of the data in figure 3 can be seen that the result can be approximated by an exponential decay. As can be expected for such a dependency, increasing the amount of projected patterns leads to a high initial gain

in reconstruction quality and converges to a best possible reconstruction quality for high numbers of projected patterns. In figure 3, the following exponential function has been fitted to the data:

$$C(a_{\mathrm{rec}}^{n_{\mathrm{patterns}}})_{\mathrm{fit}} = \mathrm{e}^{-\alpha\cdot(x-b)} + c \qquad \alpha, b, c \in \mathbb{R} \tag{12}$$

The increase in reconstruction quality then follows the following equation, mapping quality increase to an interval of $[0, 1[$, where 1 indicates that the optimal reconstruction quality has been achieved:

$$1 - \frac{C(a_{\mathrm{rec}}^{n_{\mathrm{patterns}}})_{\mathrm{fit}}}{C(a_{\mathrm{rec}}^{1})_{\mathrm{fit}}} = 1 - \mathrm{e}^{-\alpha(x-1)}, \qquad \text{for } x \geq 1 \tag{13}$$

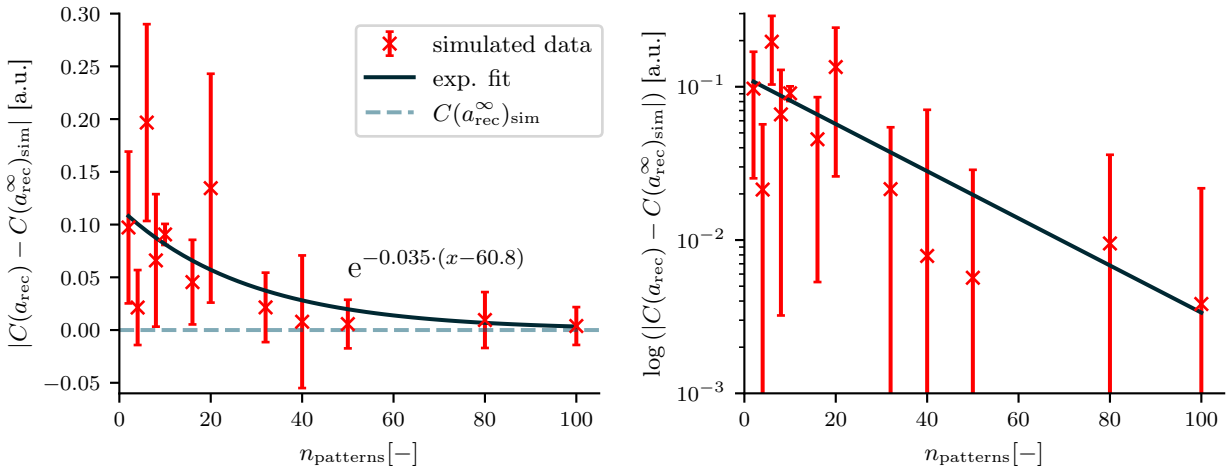

Fig. 3. *Dependence of the change in reconstruction quality and the number of projected patterns $n_{patterns}$ as a linear (left) and semilogarithmic plot (right): The presented data has been generated by reconstructing simulated measurement data with a pixel cluster size of $d_{spix,sim} = 0.4\,\mathrm{mm}$ for a defect pair for different separation distances $a_{def} \in \{0.2, 0.5, 1.5\}\mathrm{mm}$. Each data point shows the mean achieved reconstruction quality $C(a_{rec}^{n_{patterns}})$ and $\pm 1\,\sigma$ standard deviation. All data is referenced to the best achievable mean reconstruction quality $C(a_{rec}^{\infty})_{sim}$ for $n_{patterns} \to \infty$ determined by the the exponential fit shown. For the plot, $C(a_{rec}^{\infty})_{sim}$ is set to zero.*

For a best-fit factor of $\alpha = 0.035$ determined from the simulated data, this means that for projecting $n_{\mathrm{patterns}} = 50$ already $82\,\%$ of the best possible reconstruction quality is achieved. Furthermore, from the data it can be observed, that the reconstruction quality is more consistent for different defect patterns at higher number of patterns ($n_{\mathrm{patterns}} \gtrsim 50$) projected which can be seen in the lower standard deviation of the results. The overall quite high variability in the reconstruction result can be explained by the nature of the highly non-linear inverse problem which is solved here. For a higher number of patterns projected the additional information gained aids in narrowing the solution space to a point, where a more consistent result can be achieved. Nevertheless, even for a low amount of patterns projected the reconstruction quality already can be quite high but suffers from a large uncertainty whether an optimal solution has been obtained.

In order to verify these findings against real measurement data, several measurements with a pixel cluster sizes of $d_{\mathrm{spix}} \in \{0.4, 0.8\}\mathrm{mm}$ and a pattern fill factor of $\beta = 0.5$ have been performed. The achieved reconstruction quality results from those measurements together with the fit established in figure 3 can be found in figure 4. Here it can be seen, that the distribution of the achievable reconstruction quality closely matches the results on simulated data and the distribution obtained from the measured data fits the exponential fit function equally well as the reconstruction results for simulated data.

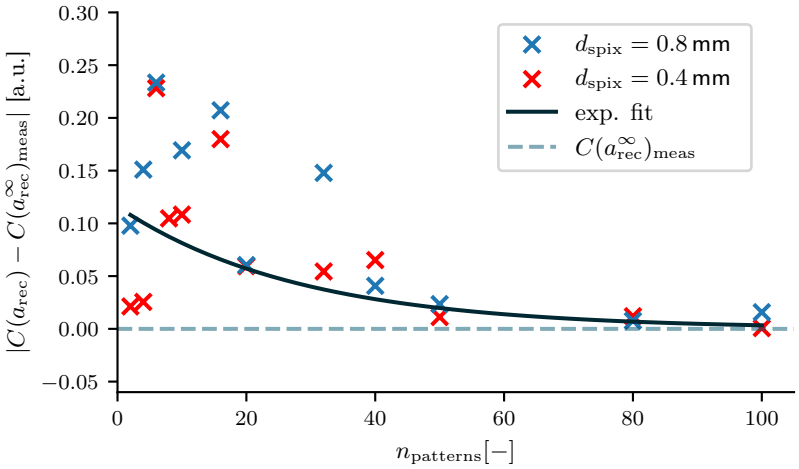

Fig. 4. *Fit model quality for measured data: In this plot the exponential reconstruction quality improvement model from figure 3 is shown next to actually achieved reconstruction quality data points from reconstruction the whole ROI as shown in figure 2. The measured data points have been rescaled to converge to the same best reconstruction quality* $C(a_{rec}^{\infty})_{sim}$ *as for the simulated data.*

7. Summary and Outlook

In this work we have given an introduction into the experimental extension of photothermal super resolution reconstruction for the thermographic detection of internal defects. This extension allows a drastic decrease in necessary measurement duration by the projection of fully two-dimensionally structured pixel patterns using a high-power DMD-based laser projector. With the use of a specifically designed forward solution to the underlying inverse problem, we have been able to examine the achievable reconstruction quality in dependence of the number of patterns projected by performing a reconstruction on several sets of generated synthetic measurement data. Ideally this number is kept as small as possible in order to achieve the shortest possible measurement times and the highest testing throughput.

Using simulated data, we have found that the projection of ≈ 50 different pixel patterns resembles a good trade-off between achievable reconstruction quality and measurement effort for the investigated ROI. This value and the overall dependence of the achievable reconstruction quality on the number of patterns projected has subsequently been verified using real measurement data from the same ROI. While projecting around 50 different pixel patterns is necessary to achieve close to the optimal reconstruction quality with reasonable efforts, a much smaller number of measurements already offers a reasonable reconstruction of the internal defect structure.

While the detection and separation of the defects already works quite well, the reconstruction of the defect shape on measured data is still lacking. The fact that the shape reconstruction works significantly better on the simulated data shows that the current underlying model of the photothermal super resolution reconstruction method - which is only a simplifying approximation of the underlying physics - needs to be refined in order to improve the ability of accurately reconstructing the defect shape. This is in conjunction with a further speed-up of the method by employing machine learning based inversion techniques a topic of current research.

References

[1] Peter Burgholzer, Thomas Berer, Jürgen Gruber, and Günther Mayr. Super-resolution thermographic imaging using blind structured illumination. *Applied Physics Letters*, 111(3):031908, July 2017.

[2] Samim Ahmadi, Julien Lecompagnon, Philipp Daniel Hirsch, Peter Burgholzer, Peter Jung, Giuseppe Caire, and Mathias Ziegler. Laser excited super resolution thermal imaging for nondestructive inspection of internal defects. *Scientific Reports*, 10(22357), 2020.

[3] Julien Lecompagnon, Samim Ahmadi, Philipp Hirsch, Christian Rupprecht, and Mathias Ziegler. Thermographic detection of internal defects using 2D photothermal super resolution reconstruction with sequential laser heating. *Journal of Applied Physics*, 131(18), May 2022.

[4] Kevin Cole, James Beck, A. Haji-Sheikh, and Bahman Litkouhi. *Heat Conduction Using Greens Functions*. CRC Press, July 2010.

[5] Markus Haltmeier, Michael Sandbichler, Thomas Berer, Johannes Bauer-Marschallinger, Peter Burgholzer, and Linh Nguyen. A sparsification and reconstruction strategy for compressed sensing photoacoustic tomography. *Acoustical Society of America*, 143(6):3838–3848, June 2018.

[6] Stephen Boyd, Neal Parikh, Eric Chu, Borja Peleato, and Jonathan Eckstein. Distributed Optimization and Statistical Learning via the Alternating Direction Method of Multipliers. *Foundations and Trends® in Machine Learning*, 3(1):1–122, 2011.

[7] Julien Lecompagnon, Samim Ahmadi, Philipp Hirsch, Christian Rupprecht, and Mathias Ziegler. Investigations on photothermal super resolution reconstruction using 2D-structured illumination patterns. In Masafumi Kimata, Joseph A. Shaw, and Christopher R. Valenta, editors, *SPIE Future Sensing Technologies 2021*, volume 11914, pages 124–131. International Society for Optics and Photonics, SPIE, 11 2021.

[8] Julien Lecompagnon, Philipp Hirsch, Christian Rupprecht, and Mathias Ziegler. Thermographic testing using 2D pseudo-random illumination and photothermal super resolution reconstruction. In Arantza Mendioroz and Nicolas P. Avdelidis, editors, *Thermosense: Thermal Infrared Applications XLIV*, volume 12109. International Society for Optics and Photonics, SPIE, May 2022.

[9] Rainer Storn and Kenneth Price. Differential Evolution - A Simple and Efficient Heuristic for global Optimization over Continuous Spaces. *Journal of Global Optimization*, 11(4):341–359, 1997.